Steel and Composite Structures, *Vol. 36, No. 5 (2020) 569-586*
DOI: https://doi.org/10.12989/scs.2020.36.5.569

Behavior and resistance of truss-type shear connector for composite steel-concrete beams

Jerfson M. Lima[1a], Luciano M. Bezerra[*1], Jorge Bonilla[2b],
Ramon S.Y.R.C. Silva[1c] and Wallison C.S. Barbosa[1d]

[1]*Department of Civil and Environmental Engineering, University of Brasília, Brazil*
[2]*Department of Applied Mathematics, University of Ciego de Ávila, Cuba*

(*Received March 10, 2019, Revised August 10, 2020, Accepted August 10, 2020*)

Abstract. The behavior of composite steel-concrete beams depends on the transmission of forces between two parts: the concrete slab and the steel I-beam. The shear connector is responsible for the interaction between these two parts. Recently, an alternative shear connector, called Truss Type connector, has been developed; it aligns efficient structural behavior, fast construction and implementation, and low cost when compared to conventional connectors applied in composite structures. However, there is still a lack of full understanding of the mechanical behavior of the Truss Type connector, due to its novelty. Thus, this study aims to analyze the influence of variation of geometric and physical parameters on the shear resistance of the Truss Type connector. In order to investigate those parameters, a non-linear finite element model, able to simulate push-out tests of Truss Type connectors, was specifically developed and validated with experimental results. A thorough parametric study, varying the height, the angle between rods, the diameter, and the concrete strength, was conducted to evaluate the shear resistance of the Truss Type connector. In addition, an equation to predict the resistance of the original Truss Type shear connector was proposed.

Keywords: composite structures; truss type connector; finite element modeling; push-out test

1. Introduction

Composite structural elements consist of a combination of materials with the purpose of their main resistance characteristics are optimized. For example, composite steel and concrete beams are designed so that, the steel is primarily responsible for supporting tension stresses and the concrete for supporting compressive stresses. In general, the steel-concrete composite beams present greater rigidity and lower cost when they are compared to equivalent structural steel or reinforced concrete beams, thus justifying their use.
The efficiency of the composite structure depends on the interaction between the materials. The communication between the materials of the composite structure is guaranteed by the mechanical action, friction and adhesion of the components. The mechanical action is performed by the shear connectors, responsible for transferring the stresses at the steel-concrete interface. In the case of composite beams, the shear connectors resist the shear forces at the steel-concrete interface and prevent the uplift between the steel I-beam and the concrete slab (Araújo *et al*. 2016, Lam 2007).
Most shear connectors have constraints in terms of fabrication, installation, and structural behavior (Shariati *et al.* 2016). The headed stud, for example, the most used connector in the steel-concrete composite structures (Cândido-Martins *et al*. 2010, Kim *et al*. 2016, Bonilla *et al*. 2018) may suffer fatigue damage when they are subjected to cyclic loads. Moreover, studs require high power equipment to execute the weld at their base (Veríssimo *et al*. 2006). The Truss-Type (TT) shear connector (Fig. 1) was developed by Barbosa (2016) as an alternative to headed studs. It can be applied to composite concrete-steel beams and was registered in the Brazilian National Institute of Industrial Property, under the number: BR302016002949-0.

The TT shear connector can be manufactured with a regular CA-50 steel bar, used in reinforced concrete structures. Its installation is performed by welding its base on the flange of the steel beam. The connector is embedded in the concrete slab. Fillet welds are carried out on both sides along the horizontal legs of the connector (see Fig. 1). From the structural point of view, the TT shear connector offers to the connection higher resistance values for longitudinal shear forces and effectiveness in preventing the longitudinal slip and uplift at the interface between the steel beam and concrete slab. In addition, this type of connector offers a lower cost of production and does not require specific welding equipment for its installation like electric guns operated with high electric power for the installation

*Corresponding author, Professor
E-mail: lmbz@unb.br
[a]Ph.D. Student
E-mail: jerfsonlima2009@hotmail.com
[b]Professor
E-mail: jorgedbr@unica.cu
[c]Senior Engineer
E-mail: ramon@unb.br
[d]Associate Professor
E-mail: wallison.barbosa@ifg.edu.br

ISSN: 1229-9367 (Print), 1598-6233 (Online)

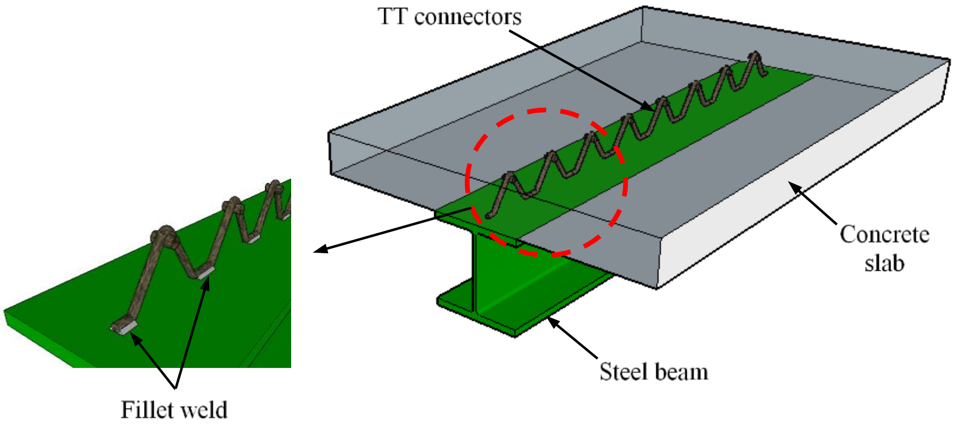

Fig. 1 Truss-Type Shear connector

of headed studs. For more details on the construction and use of TT shear connectors, see Bezerra *et al*. (2018).

The performance of the shear connector is often investigated with the push-out test, in which the shear resistance of the connector, load-slip behavior, and uplift are determined. However, when it is desired to test several push-out models, the time and economic cost spent are high. Hence, the use of finite element (FE) modeling can be very helpful to understand the behavior of shear connectors and connections (Ellobody and Young 2006). As an example of the above, some researches, among others, on this subject are highlighted. Lam and Ellobody (2005) developed nonlinear numerical models in finite elements to simulate the behavior of the headed stud shear connector in composite beams. In such models, the shear resistance of the connection, the load-slip behavior of the headed studs, and the rupture modes obtained by the finite element analyses showed very good agreement with the experimental results. Using a non-linear finite element model of the push-out tests, Nguyen and Kim (2009) performed an extensive parametric study to evaluate the effect of the changes in the diameter of the headed stud, and the concrete strength on the stud shear resistance and ductility of a composite beam with a solid slab. Qureshi and Lam (2012) and Qureshi *et al*. (2011) in their searches developed a non-linear finite element model to study the behavior of the connection to the stud bolt connector in composite beams with profiled sheeting. Qi *et al*. (2017) developed push-out tests and FE analysis to investigate the effect of the damage degree and location on the static behavior and shear resistance of stud connectors. Han *et al*. (2017) evaluated the connection of composite beams with crumb rubber concrete slabs instead, through the development of a non-linear numerical model in finite elements. Likewise, Bezerra *et al*. (2018) using a non-linear three-dimensional finite element model simulated the TT shear connector behavior providing numerical results consistent with experimental tests. In the last past years, numerical modeling has been also widely used to analyze the behavior of full-scale steel-concrete composite beams, obtaining accurate results in agreement with real tests (Ban *et al*. 2016, Turmo *et al*. 2015, Xing *et al*. 2016, Zona and Ranzi 2014).

This paper aims to develop an efficient non-linear finite element numerical model to make a parametric study of the resistance of TT shear connector in composite beams with a solid slab. In order to develop and analyze the numerical model; the finite element program ABAQUS (2014a) was used. Calibration and validation of the model were achieved through experimental results obtained by Barbosa (2016). The parametric study was carried out to evaluate the shear resistance of the TT connector, varying: (1) its height, (2) the angle of the aperture between its legs, (3) the connector diameter, and (4) the influence of the concrete strength of the slab. With the numerical results, a statistical analysis was applied to obtain an expression that rules the nominal resistance of the TT shear connector.

2. Geometry of the push-out test

In order to calibrate and validate the numerical model; push-out specimens tested by Barbosa (2016) were used in this study. Barbosa´s experiments were based on the standard push-out test model found in the Eurocode-4 (2004), the standard that regulates this test. Only one modification was made in relation to the usual specimen dimensions: 100 mm was added in the length of the slabs, for better accommodation of the TT connectors. It resulted in the application of another crossbar to the reinforcement of the slab. Figs. 1 and 2 illustrate the specimen geometry. Barbosa (2016) tested specimens using TT connectors with diameters (*d*): of 8, 10, and 12.5 mm. To avoid uplift, the TT connector was conceived with a piece of 40 mm in length and 16 mm in diameter welded on its top angle (Fig. 2). Each model for the push-out test has 8 TT connectors (see Figs. 2-3(a)).

3. Finite element model

The numerical simulation of the push-out test with TT connectors was developed using ABAQUS (2014a) software. The FE model encompasses the connectors, concrete slab, steel I-beam, and reinforcement bars of the slab. The interaction between those components is

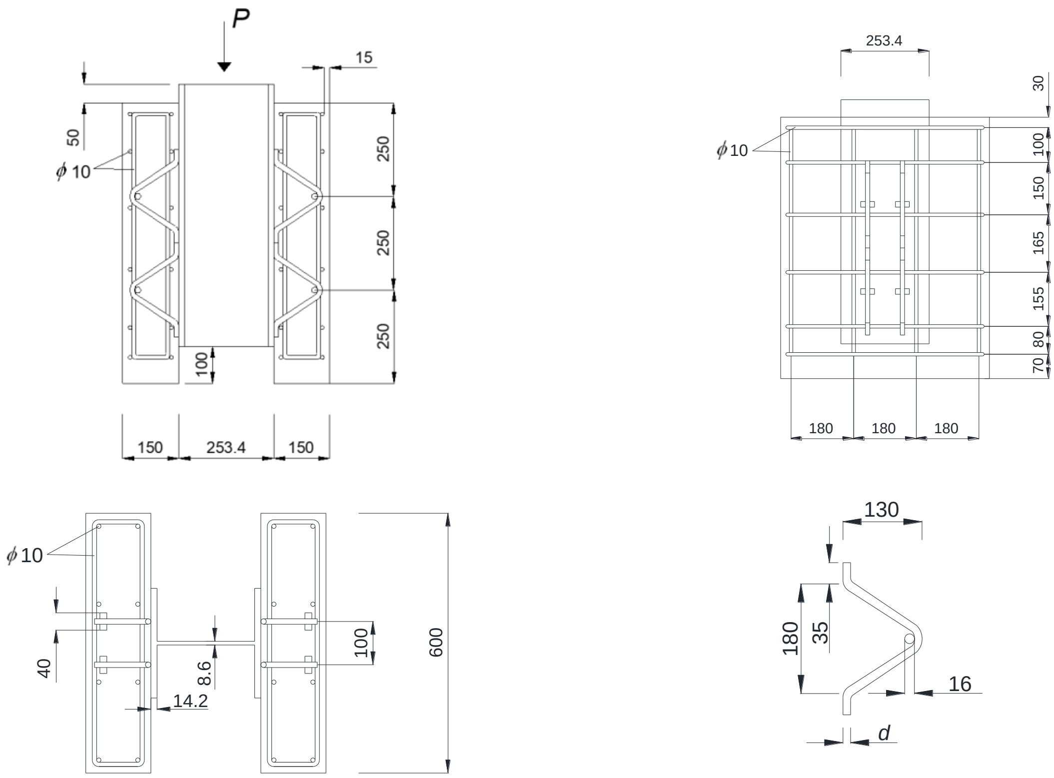

Fig. 2 Detailed geometry of the experimental model for test of TT connectors (mm)

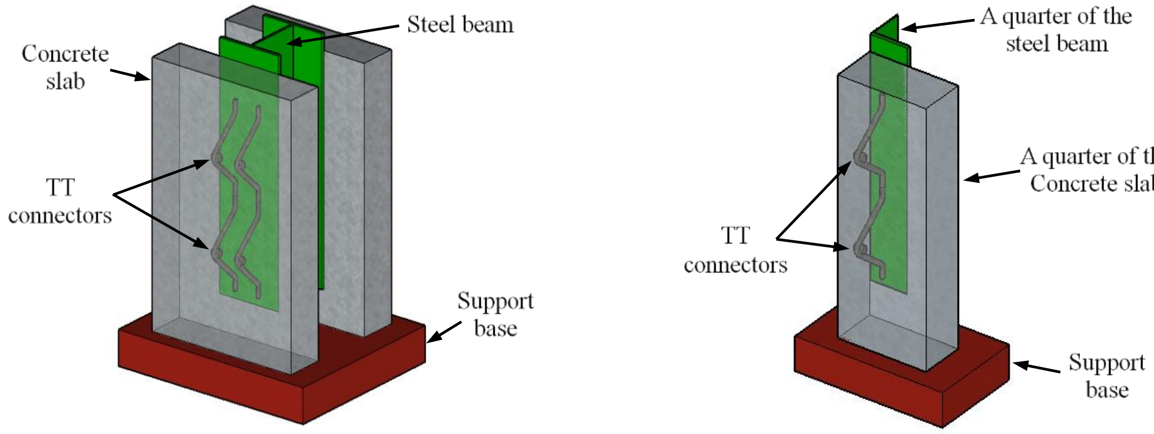

(a) Full view of push-out test specimen

(b) A quarter of push-out test specimen

Fig. 3 Views of the push-out specimen geometry

extremely important to simulate the push-out test. All sources of non-linearity (materials and contact) were considered in the analysis. In order to reduce the computational cost during the numerical analysis; the geometry symmetry of the push-out test was considered. Therefore, only a quarter of the experimental specimen was modeled (Fig 3). Due to this consideration, special boundary conditions were applied.

3.1 Finite element mesh and types

Each part of the model was modeled separately, thus establishing independent meshes. ABAQUS (2014b) states that for the solid part modeling, the C3D8R element (8-node hexadecimal three-dimensional element with reduced integration) available in the ABAQUS (2014a) finite element library offers better results and lower computational cost during the analysis. However, the complex geometry of the TT shear connector did not allow this finite element to be applied throughout the whole push-out model.

The slab was modeled using two types of elements. In the region close to the connectors, C3D8R elements were used. However, in the region around the TT connectors, due

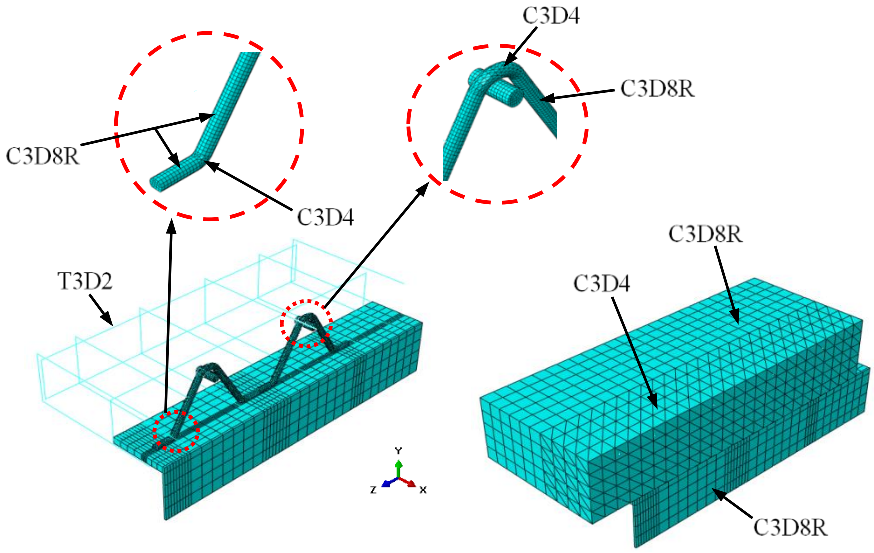

Fig. 4 Mesh and types finite elements

Table 1 Summary of the finite element model, element types, and meshes

Parts of the model	Element type	Number of elements	Number of nodes
Slab	C3D8R	750	1092
	C3D4	26207	5431
TT shear connector	C3D8R	1097	1762
	C3D4	1008	318
Steel I-beam	C3D8R	663	1440
Reinforcement bars of the slab	T3D2	698	704

to complex geometry, C3D4 elements (tetrahedral three-dimensional element with four nodes) were applied. The connector was modeled with C3D8R and C3D4 elements, the steel I-beam only with C3D8R elements; and the reinforcement bars of the slab with truss elements with two nodes (T3D2). The distribution of the elements in the model is shown in Fig. 4. The finite elements used in the model, present in the ABAQUS (2014a) finite element library, enable non-linear analyses, including contact, large deformations, plasticity, and failure. The calibration of the model indicated that refinement of the finite element mesh in regions close to the connectors produce accurate results. This fact is explained by the high concentration of stresses in those regions. The maximum and minimum sizes of the mesh elements were 30 and 5 mm, respectively.

Table 1 presents in detail the number of nodes and the finite element types used in each part of the model. For this finite element mesh configuration, the average processing time was 19 hours, on a computer with an Intel Core i5-2500 processor, processing frequency of 3.5 Gigahertz, and 8 Gigabytes of RAM memory.

3.2 Constraints and contact interactions

Appropriate constraints and contact interactions were applied to simulate the interface between the parts of the model. Barbosa (2016) found that after the rupture of the experimental push-out specimen, the connection between the connector and the steel beam remained intact. For this reason, tie restrictions have been applied between the lower surface of the horizontal legs of the connector and the upper surface of the steel I-beam flange. Such tie constrains unify the displacements of the nodes of these two surfaces eliminating the slip between them. Based on Bezerra *et al.* (2018), tie constraints in-between connector-concrete interface were also assumed (Fig. 5(a)). Nguyen and Kim (2009), in their studies with headed studs, affirm that the use of the tie in this situation constitutes an adequate approximation. The reinforcement bars of the slab were embedded in the concrete slab, with the application of the embedded constraint. This restriction ensures the combined behavior of the bars with the concrete slab, neglecting the sliding of the bars.

In experimental push-out tests, it is common to apply a lubricant on the upper surface of the steel I-beam flange (Eurocode-4 2004). In the numerical model, a contact interaction was applied to the flange surfaces of the steel I-beam and the slab (Fig. 5(b)). The properties of the contact interaction consisted of frictionless tangential behavior and normal hard behavior. The frictionless tangential property allows the free slip between the surfaces and the normal hard property prevents penetration between the surfaces.

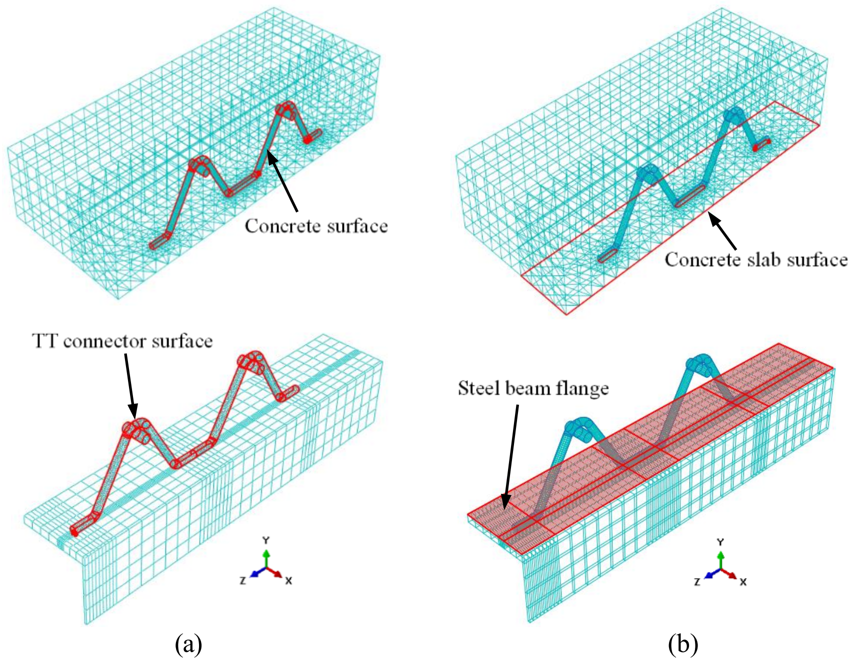

Fig. 5 Constraints and contact interactions: (a) Surfaces in tie constrain between concrete and TT connectors. (b) Surfaces in contact interaction between steel beam flange and concrete slab

3.3 Boundary conditions and loading

In order to succeed in the geometric simplification of the model, the boundary conditions of the symmetry were applied (Fig. 6). All nodes along Surface 1 were restricted from moving in the X-direction. On the surface of the steel I-beam web section (Surface 2), the displacements of all nodes were prevented in the Y-direction. The boundary condition for the push-out test consisted of restricting the displacements of the nodes of Surface 3 in the Z-direction. The load was applied uniformly in the steel I-beam cross-section, as seen in Fig. 6.

3.4 Analysis method

In this study, the explicit dynamic analysis method was applied. Although it is a dynamic method, it can be applied to analyze static models as well, since it is provided that the effects of inertia are controlled by the slow application of load. The explicit dynamic method is very effective in the analysis of complex models involving material damage, large deformations, and contact interactions between different parts; hence, it is appropriate to analyze push-out models. Several researchers applied this method to simulate push-out tests and obtained good results (Bezerra *et al*. 2018, Kim *et al*. 2017, Pavlovic *et al*. 2013, Paknahad *et al*. 2018, Qureshi and Lam 2012, Qureshi *et al*. 2011, Shariati *et al*. 2016, Xu *et al*. 2014, Zheng *et al*. 2019). In this paper, the load application rate was chosen so that, during the analysis, the effects of inertia were minimal. The slowly loading was used by applying a constant velocity of 0.25 mm/s, as used by Qureshi and Lam (2012).

3.5 Constitutive model for concrete

In order to model the concrete; it was used the Concrete Damage Plasticity Model (CDPM), available in ABAQUS (2014a) material library. This constitutive model is appropriate for materials that have different tension and compressive strength; in addition, it links the theory of plasticity with the damage mechanics, being able to numerically simulate the degradation of concrete stiffness and failure. The failure mechanisms considered are based on tensile cracking and compression crushing of concrete. The CDPM assumes a non-associative plastic flow rule, using Drucker-Prager's hyperbolic function to define the potential flow. The plastic parameters of the CDPM model used were (Alfarah *et al*. 2017, Lopez-Almansa *et al*. 2014): (a) an angle of dilation (φ) of 13°, (b) Ratio between the magnitudes of deviatoric stress in uniaxial tension/compression K_c = 0.7, (c) Eccentricity of the plastic potential surface ϵ = 0.1, and (d) The ratio between biaxial and uniaxial compressive yield strengths (f_{b0}/f_{c0}) of 1.16.

The concrete uniaxial compression behavior is shown in Fig. 8(a). The ascending part (parts 1 and 2) was based on the recommendations of the *FIB Model Code* 2010 (2012), while the descending part (part 3) was assumed to be the softening function developed by Krätzig and Pölling (2004). The f_{cm} represents the average compressive strength, wherein ε_{cm} is the corresponding strain, which displays the peak of the stress-strain curve. The E_0 is the concrete secant Young's modulus. The f_{cm} (MPa) and E_0 (MPa) were obtained from the *FIB Model Code* 2010 (2012)

$$f_{cm} = f_{ck} + 8 \tag{1}$$

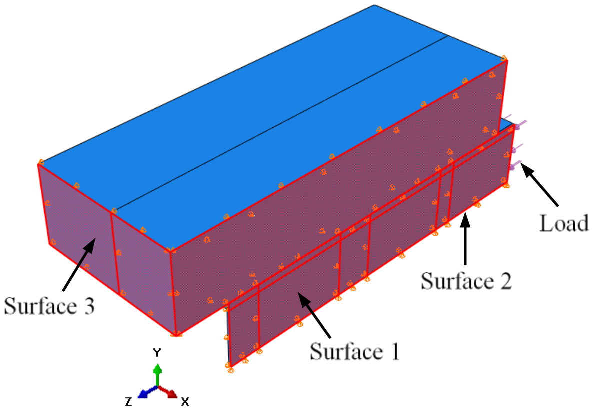

Fig. 6 Loading and boundary conditions of the push-out test

$$E_0 = \left(0.8 + 0.2\frac{f_{cm}}{88}\right)E_{ci} \tag{2}$$

$$E_{ci} = 10000\, f_{cm}^{\frac{1}{3}} \tag{3}$$

Where f_{ck} (MPa) is the characteristic strength of concrete and E_0 (MPa) is the initial modulus of elasticity. ε_{cm} is selected according to the concrete strength class, see *FIB Model Code* 2010 (2012).

Part-1 of the stress-strain curve in Fig. 8(a) is under compression and extends up to the stress $0.4f_{cm}$. This part is linear and governed by Eq. (4). Part-2 also in compression extends from $0.4f_{cm}$ to f_{cm} and corresponds to Eq. (5) – see *FIB Model Code* 2010 (2012).

$$\sigma_{c(1)} = E_0 \varepsilon_c \tag{4}$$

$$\sigma_{c(2)} = \frac{E_{ci}\dfrac{\varepsilon_c}{f_{cm}} - \left(\dfrac{\varepsilon_c}{\varepsilon_{cm}}\right)^2}{1 + \left(E_{ci}\dfrac{\varepsilon_{cm}}{f_{cm}} - 2\right)\dfrac{\varepsilon_c}{\varepsilon_{cm}}} f_{cm} \tag{5}$$

Part-3 in softening compression is given by

$$\sigma_{c(3)} = \left(\frac{2 + \gamma_c f_{cm}\varepsilon_{cm}}{2 f_{cm}} - \gamma_c \varepsilon_c + \frac{\varepsilon_c{}^2 \gamma_c}{2\varepsilon_{cm}}\right)^{-1} \tag{6}$$

$$\gamma_c = \frac{\pi^2 f_{cm}\varepsilon_{cm}}{2\left[\dfrac{G_{ch}}{l_{eq}} - 0.5 f_{cm}\left(\varepsilon_{cm}(1-b) + b\dfrac{f_{cm}}{E_0}\right)\right]^2} \tag{7}$$

$$b = \frac{\varepsilon_c{}^{pl}}{\varepsilon_c{}^{ch}} \tag{8}$$

The G_{ch} (Eq. (7)) is the concrete crushing energy per unit area and l_{eq} is the characteristic length of the finite element used to model the concrete; it is obtained by the relation between the volume and the area of the largest surface of the finite element used. The maximum strain value is adopted so that the area under the curve (Fig. 8(a)) is equal to the relation G_{ch}/l_{eq} (Krätzig and Pölling, 2004).

In Fig. 8(a), d_c is the compression damage (Eq. (15)); $\varepsilon_c{}^{ch}$ and $\varepsilon_{0c}{}^{el}$ are the crushing and elastic undamaged components of strain; $\varepsilon_c{}^{pl}$ and $\varepsilon_c{}^{el}$ are the plastic and elastic damaged components. In Eq. (8), it can initially be assumed b = 0.9 (Alfarah *et al*. 2017). After calculating the strains $\varepsilon_c{}^{pl}$ and $\varepsilon_c{}^{ch}$, an average value for b is obtained and compared with the initial value. Interactive calculations are performed until convergence is achieved.

The uniaxial behavior of the tensile concrete is shown in Fig. 8(b). The ascending path is taken as linear-elastic and the descending path is specified in terms of fracture energy, based on the exponential curve derived from the Cornelissen *et al*. (1986) (Fig. 7).

In Fig. 7, f_{tm} is the tensile strength, G_f is the fracture energy per unit area, w_c is the critical crack opening. f_{tm} (MPa) and G_f (N/mm) are given by (FIB Model Code 2010, 2012)

$$f_{tm} = 0.3016\, f_{ck}{}^{2/3} \tag{9}$$

$$G_f = 0.073\, f_{cm}{}^{0.18} \tag{10}$$

In Eq. (10), f_{cm} is expressed in MPa. Based on the fracture energy, Oller (1988) defines that the concrete crushing energy (G_{ch}) can be obtained according to Eq. (11).

$$G_{ch} = \left(\frac{f_{cm}}{f_{tm}}\right)^2 G_f \tag{11}$$

The exponential expression proposed by Cornelissen *et al*. (1986) relates tension to crack opening (Eq. (12)). In this expression, $\sigma_t(0) = f_{tm}$ and $\sigma_t(w_t) = 0$, meaning: when the crack opening is zero, the strength is maximum; and when the crack opening is maximum, the strength is zero.

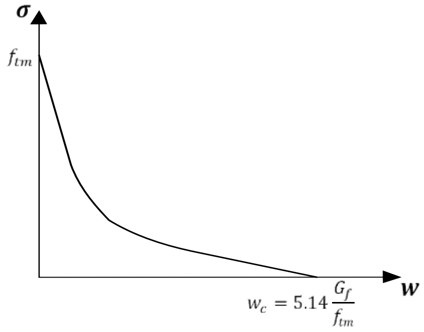

Fig. 7 Softening in the tension in terms to the crack opening

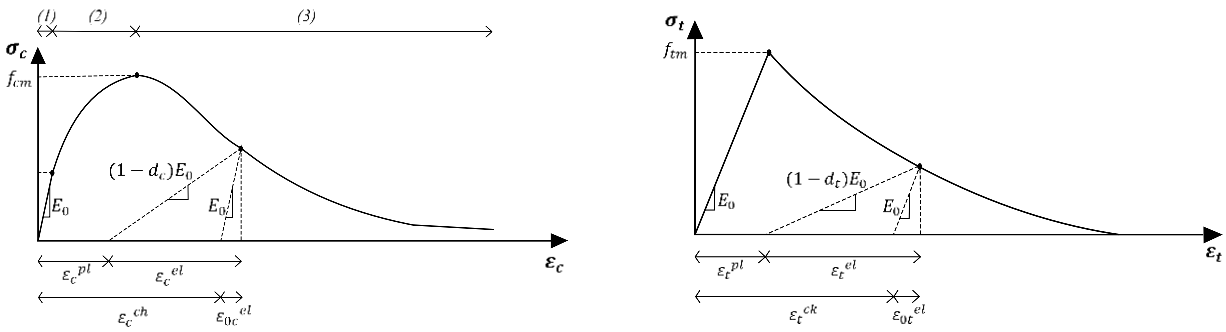

(a) Compression (b) Tension

Fig. 8 Concrete uniaxial behavior

c_1 = 3, c_2 = 6.93, and w_c can be calculated by Eq. (13) (Cornelissen *et al*. 1986).

$$\frac{\sigma_t(w)}{f_{tm}} = \left[1+\left(c_1\frac{w}{w_c}\right)^3\right]e^{-c_2\frac{w}{w_c}} - \frac{w}{w_c}\left(1+c_1^3\right)e^{-c_2} \quad (12)$$

$$w_c = 5.14\frac{G_f}{f_{tm}} \quad (13)$$

The softening in the tension (Fig. 8(b)) can also be defined in terms of the strain, from Eq. (14) (Alfarah *et al*. 2017).

$$\varepsilon_t = \varepsilon_{tm} + \frac{w}{l_{eq}} \quad (14)$$

The ε_{tm} is the strain corresponding to the tension strength (f_{tm}). Fig. 8(b) shows the tension-strain curve applied.

Similar to the compression law, see Fig. 8(a), d_t is the tension damage; ε_t^{ck} and ε_{0t}^{el} are the cracking and elastic undamaged components of strain components; ε_t^{pl} and ε_t^{el} are the plastic and elastic damaged components. In the implementation of the uniaxial compression and tension laws in the CDPM, the stains ε_c^{ch} and ε_t^{ck}, respectively, were applied. In this study, the concrete damage evolution was based on the methodology developed by Alfarah *et al*. (2017). The authors proposed that the compression (d_c) andtension (d_t) damage variables can be obtained by Eq. (15) and (16).

$$d_c = 1-\frac{1}{2+a_c}\left[2\left(1+a_c\right)e^{\left(-b_c\varepsilon_c{}^{ch}\right)} - a_c e^{\left(-2b_c\varepsilon_c{}^{ch}\right)}\right] \quad (15)$$

$$d_t = 1-\frac{1}{2+a_t}\left[2\left(1+a_t\right)e^{\left(-b_t\varepsilon_t{}^{ck}\right)} - a_t e^{\left(-2b_t\varepsilon_t{}^{ck}\right)}\right] \quad (16)$$

In which

$$a_c = 7.873;\ a_t = 1;\ b_c = \frac{1.97\left(f_{ck}+8\right)}{G_{ch}}l_{eq};\quad b_t = \frac{0.453 f_{ck}{}^{2/3}}{G_f}l_{eq} \quad (17)$$

Figs. 9 and 10 illustrate the assumed uniaxial model of concrete behavior and the evolution of the damage parameters (d_c and d_t) in terms of the crushing (ε_c^{ch}) and cracking (ε_t^{ck}) strains, respectively, for a concrete with f_{cm} = 34 MPa.

3.6 Constitutive model for steel

In this study, a constitutive elastic-plastic model was used to model steel in the TT shear connector, I-beam, and slab reinforcement bars. This constitutive model is found on

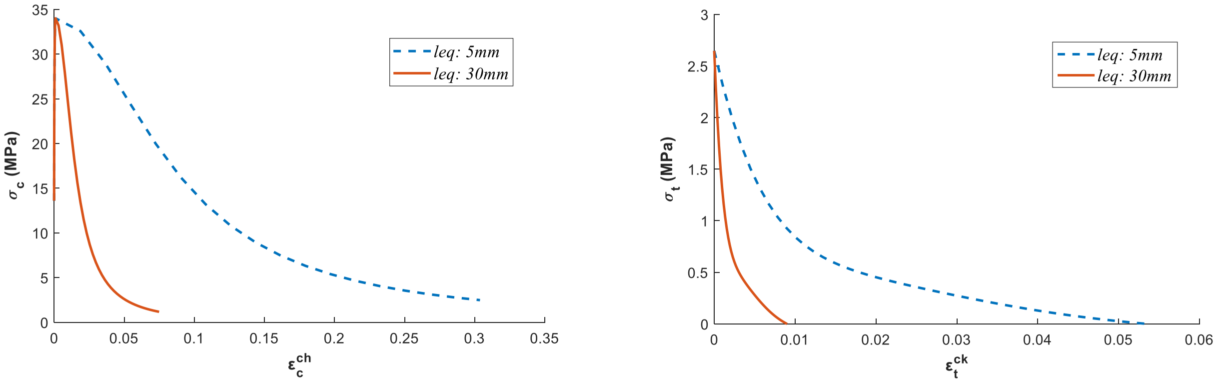

(a) Compression-crushing strain curve (b) Tension-cracking strain curve

Fig. 9 Concrete uniaxial behavior with f_{cm} = 34 MPa

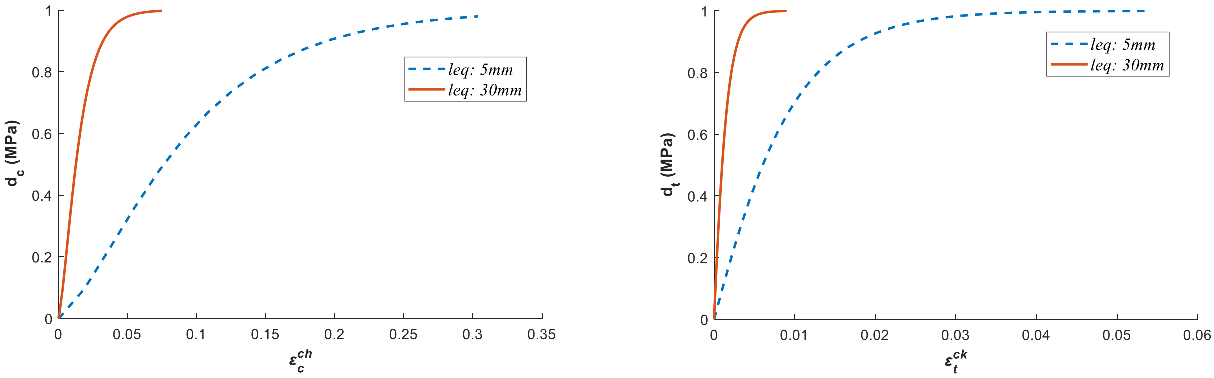

(a) Crushing damage-crushing strain curve (b) Cracking damage-cracking strain curve

Fig. 10 Evolution of the damage parameters with f_{cm} = 34 MPa

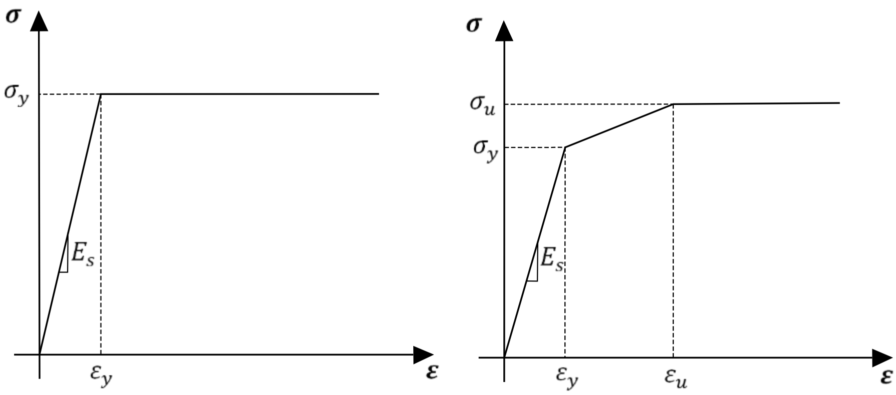

(a) Bi-linear (b) Tri-linear

Fig. 11 Stress-strain relationship for steel: (a) Bi-linear; (b) Tri-linear

the ABAQUS (2014a) material library named as PLASTIC. The PLASTIC model adopts the Von Mises yielding criterion, with associative flow rule, ideal for the ductile materials modeling such as steel. The uniaxial behavior implemented in the model consisted of the bi-linear and tri-linear stress-strain relationships. For minor state of stress, like in the steel I-beam flange and slab reinforcement; the bi-linear stress-strain curve was adopted (Fig. 11(a)). For major state of stress going into yielding, as in the TT connectors, the tri-linear curve (Fig. 11(b)) was utilized. A more refined stress-strain relationship for the TT connectors was assumed (Nguyen and Kim 2009).

Table 2 Experimental push-out models (MTT) tested by Barbosa (2016)

Model nomenclature	Details of the TT connector		
	Diameter (mm)	Height (mm)	Angle of the aperture between connector legs
MTT-8	8.0	130.0	60°
MTT-10	10.0	130.0	60°
MTT-12.5	12.5	130.0	60°

Table 3 Concrete properties of the models

E_0 (GPa)	f_{cm} (MPa)	f_{tm} (MPa)
26.0	34.0	3.6

Table 4 Properties of the steel used in the connectors, in the beam, and in the reinforcement of the slab

Steel Element	Properties	MTT-8	MTT-10	MTT-12.5
TT connector	E_s (GPa)	198.4	194.5	195.3
	σ_y (MPa)	561.2	591.6	595.3
	σ_u (MPa)	663.2	722.4	716.6
	ε_u (%)	0.6	0.6	0.6
Beam	E_s (GPa)	200.0	200.0	200.0
	σ_y (MPa)	250.0	250.0	250.0
Reinforcement of the slab	E_s (GPa)	561.2	561.2	561.2
	σ_y (MPa)	722.4	722.4	722.4

In Fig. 11, E_s is the material elastic modulus, σ_y and ε_y are the yield stress and its respective strain, σ_u and ε_u are the ultimate stress and its respective strain. The bi-linear model establishes the perfectly elastic-plastic behavior. In the tri-linear curve, the behavior is initially elastic, followed by a hardening and, immediately after that, a perfectly plastic yielding.

4. Validation of the numerical model

The finite element model validation was carried out using Barbosa's experimental push-out tests. The shear resistance of the Truss Type (TT) connector, the load-slip curve, and failure modes were verified. Table 2 presents the TT connector geometry and the nomenclature of each experimental model (MTT-d), where d is the diameter of the TT connector bar. The concrete and steel properties are described in Tables 3 and 4, respectively.

Each experimental model (MTT-d) was tested with three specimens (MTT-d#n; n=1, 2 and 3). The maximum load and the load-slip curves for each experimental test (MTT-d#n) were compared with the numerical curves obtained by the finite element analyses (FEA), as can be seen in Figs. 12 and 13. A good agreement between experimental and numerical curves is observed.

Each (MTT-d#n) specimen reached a maximum load (see Table 5) and has eight TT connectors (Figs. 2-3(a)). The average resistance per TT connector (TT-d#n) is the maximum load of each specimen (MTT-d#n) divided by 8. Table 5 presents in detail the average shear resistance (Q_{exp}) of the TT connectors obtained from the experimental push-out tests and the finite element analyses (Q_{FEA}). The greatest difference between experimental and numerical results was 5.90%. The average value of (Q_{exp}/Q_{FEA}) was 0.998, with a variation coefficient of 0.029. These results corroborate the effectiveness of the finite element model proposed to simulate the shear resistance of the TT connector.

By means of experimental observations, Barbosa (2016) and Bezerra *et al*. (2018) found that the typical rupture mode of the TT connector push-out specimens consists in the combination of the tensile rupture in one of the TT connector legs and the concrete crushing in regions near to the connector base. The experimental MTT-8 model was adopted to compare the failure mode presented in the experimental test and the numerical FE simulation. Fig. 14 shows the distribution of the Von Mises stress at the connectors at the moment that the maximum load is acting on the model. Through the deformation of the connectors, it is noted that the TT connector works predominantly on axial stress. One of the legs is subjected to tensile (T), while the other is subjected to compression (C), as indicated in Fig. 14. The highest stress values are at the base of the connectors, which are higher than the yield stress. It is also observed the beginning of the necking in the legs under tensile; it is the spot of TT connector rupture. Figs. 15 and

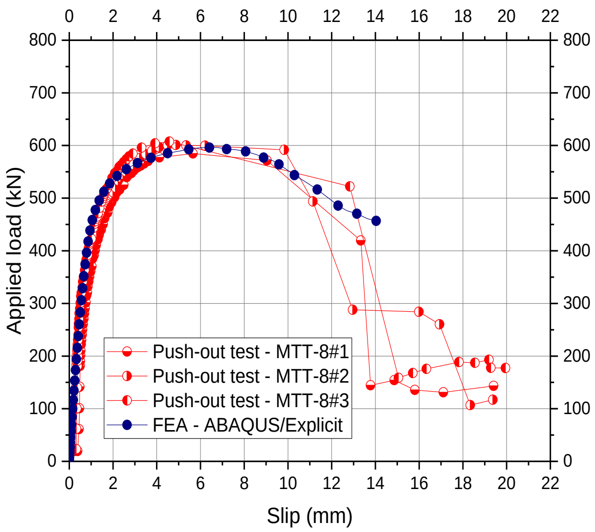

(a) Load-slip curves for the MTT-8 model

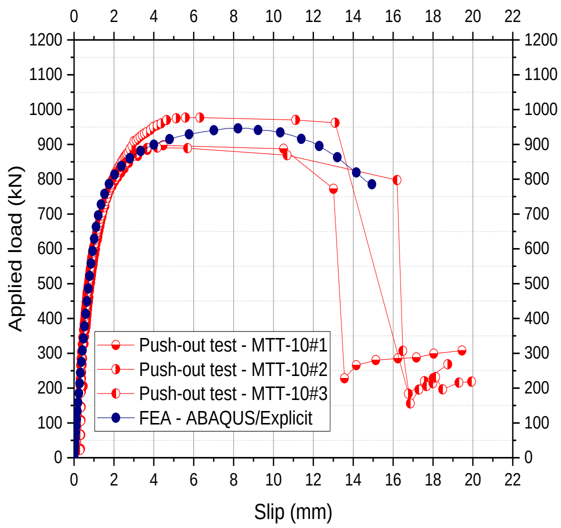

(b) Load-slip curves for the MTT-10 model

Fig. 12 Load applied versus slip for push-out specimens (MTT-8 and MTT-10)

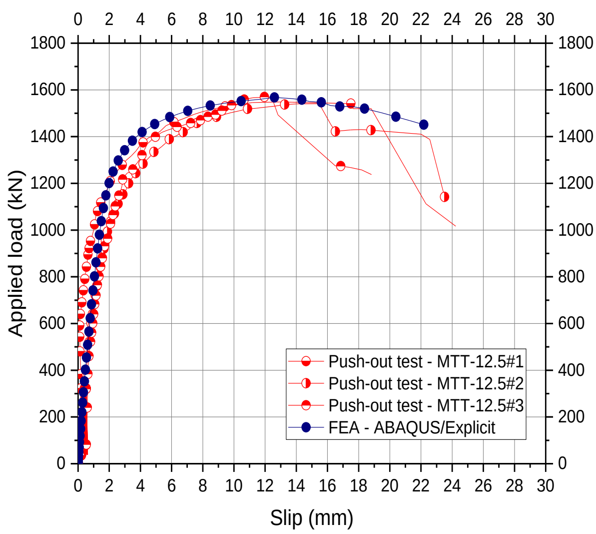

Fig. 13 Load applied versus slip for push-out specimens (MTT-12.5)

16 show the distribution of stresses and compression damage on the slab, respectively. It can be observed that spots with high stress and damage values are located near to the base of the connectors. Due to stress levels and damage values, the concrete in these sections was crushed. In view of the above, it is confirmed that there is a good agreement between the rupture modes achieved via the numerical simulation and the one visualized experimentally (Fig. 17).

Fig. 17 shows a section on the connector alignment of the MTT-8#2 push-out experimental test after collapse. It is observed the similarity in the deformation of the connectors and also an analogy in the location of the crushing regions of the concrete between the numerical and experimental results. These results demonstrate the efficiency of the proposed finite element model to numerically simulate the behavior of the Truss Type connectors.

5. Parametric study

The TT connector geometric configuration is defined by the height (h) and the angle of the aperture between the connector legs (α). The total length (l_t) is given by the sum of the horizontal distance between the base of the legs (l_{ab}) and the length of the two horizontal legs of the connector to be welded on the I-beam flange. Each of the two horizontal legs is 35 mm long. This length was studied by Barbosa (2016). The described geometric parameters can be visualized in Fig. 18.

A parametric study was conducted to evaluate the shear resistance of the TT connector, varying (1) the height (h), (2) the angle of the aperture between legs (α), (3) the diameter (d) of the steel bar used to manufacture the TT connector, and (4) the concrete strength (f_{cm}) of the slabs. The parametric study was divided in two steps. The first step was to analyze the influence of height (h) and angle (α) on

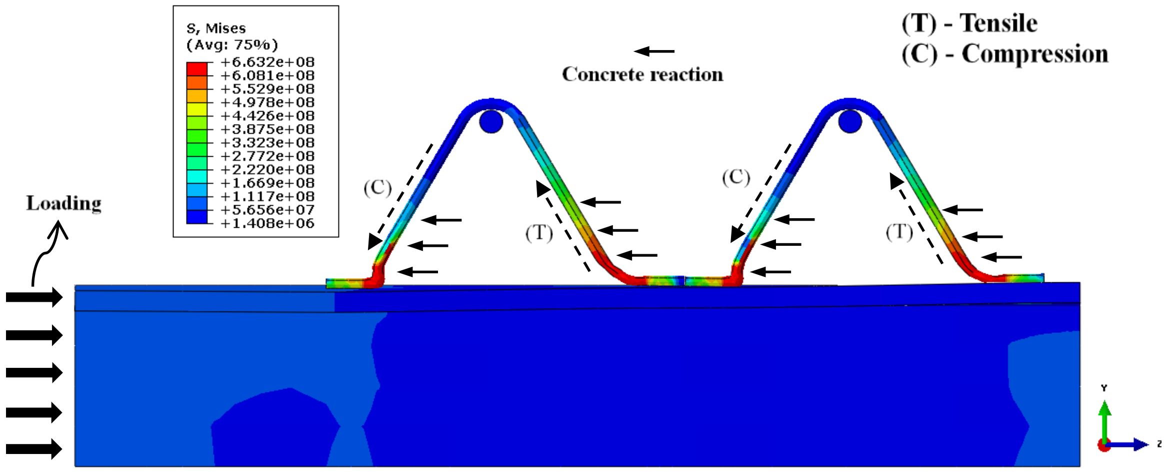

Fig. 14 Stress contours (in Pa) and TT-8 connector deformation at the moment of the maximum load of the push-out test of the MTT-8 obtained by FE analysis

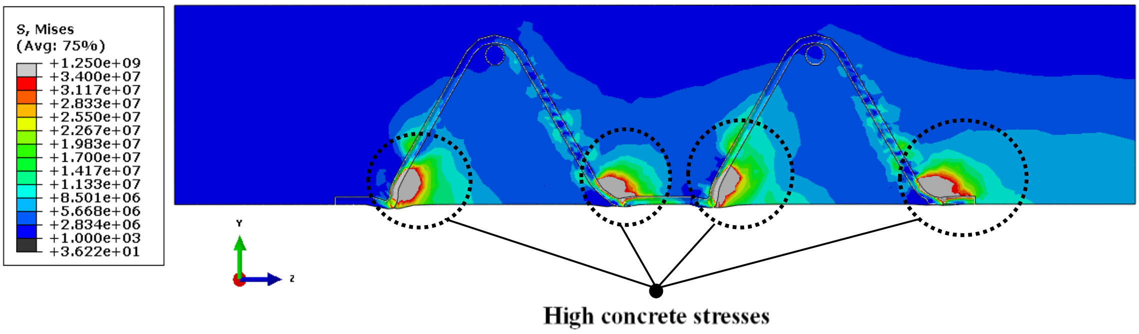

Fig. 15 Stress contours (in Pa) in the slab at the moment of the maximum load of the push-out model test of the MTT-8 obtained by FE analysis

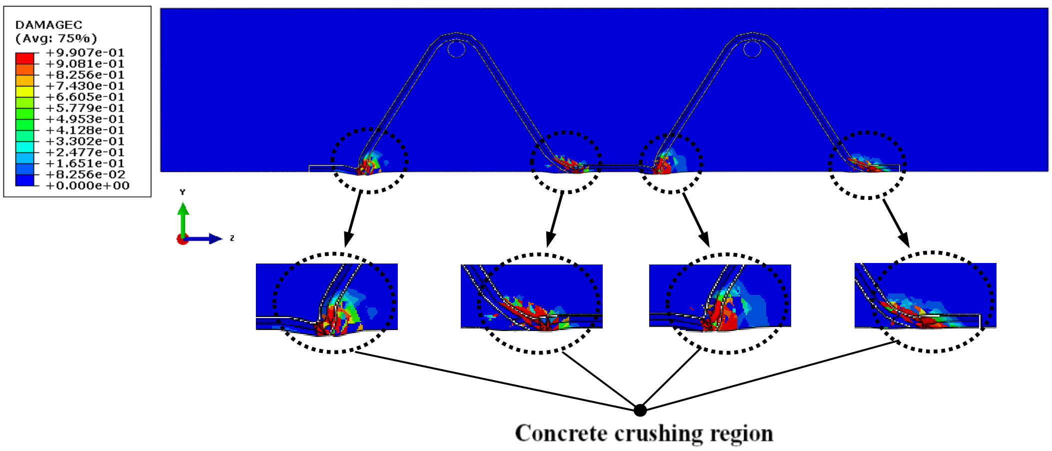

Fig. 16 Compression damage contours in the slab at the moment of the maximum load of the push-out test of the MTT-8 obtained by FE analysis

the shear resistance. The properties of the steel and concrete applied on the first step were the same as the ones applied to validate the proposed finite element model, present in Tables 3 and 4. The second step consisted of the influence of concrete strength (f_{cm}) and the bar diameter (d) utilized to manufacture the TT connection. The numerical models of the parametric study followed the standard geometry of Barbosa's experiments (Barbosa 2016), detailed in Fig. 2.

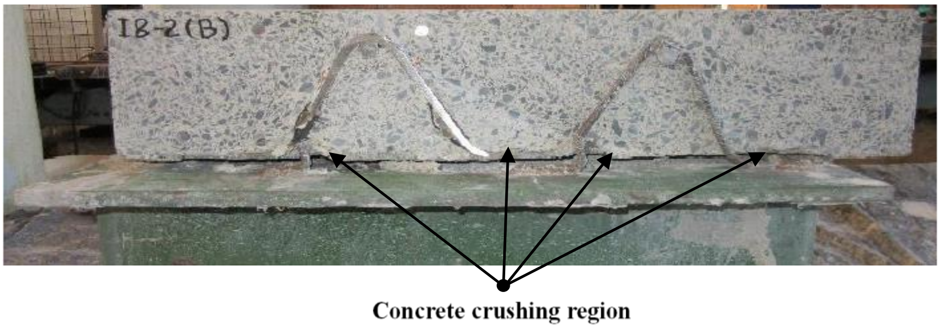

Fig. 17 Section on the connectors alignment of the MTT-8#2 specimen after the push-out test performed by Barbosa (2016)

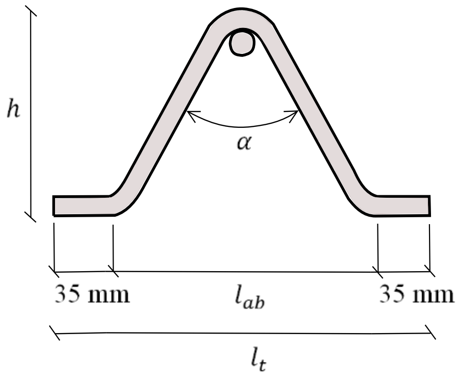

Fig. 18 TT connector geometric parameters

Table 5 Comparison between the shear resistances of the TT connectors obtained by the experimental tests and the proposed numerical FE analyses

Specimen Tested	Diameter (d) (mm)	Maximum load (kN)	TT connector	Average Q_{exp} (kN)	Q_{FEA} (kN)	Q_{exp}/Q_{FEA}
MTT-8#1		584.80	TT-8#1	73.10		0.981
MTT-8#2	8.0	601.04	TT-8#2	75.13	74.51	1.008
MTT-8#3		607.44	TT-8#3	75.93		1.019
MTT-10#1		897.04	TT-10#1	112.13		0.973
MTT-10#2	10.0	976.80	TT-10#2	122.10	115.27	1.059
MTT-10#3		890.80	TT-10#3	111.35		0.966
MTT-12.5#1		1548.64	TT-12.5#1	193.58		0.988
MTT-12.5#2	12.5	1540.80	TT-12.5#2	192.60	195.96	0.983
MTT-12.5#3		1570.00	TT-12.5#3	196.25		1.002
Mean						0.998
Coefficient of variation (CV)						0.029

Note: Q_{exp} and Q_{FEA} in this table are per TT connector (TT-d#n).

Table 6 Geometry of the connectors with the height (h) variation

TT connector nomenclature	h (mm)	α	l_{ab} (mm)	l_t (mm)
TT-12.5-H90	90.0		125.0	195.0
TT-12.5-H110	110.0	60°	150.0	220.0
TT-12.5-H130	130.0		180.0	250.0
TT-12.5-H150	150.0		205.0	275.0

Table 7 The TT connector shear resistance for different heights

TT connector	*Pult* (kN)	$Pult_{TT\text{-}12.5\text{-}H130}/Pult$
TT-12.5-H90	181.75	1.043
TT-12.5-H110	189.02	1.003
TT-12.5-H130	189.61	-
TT-12.5-H150	194.87	0.973

Pult: Shear resistance per TT connector

Table 8 Geometry of the connectors with the variation of the angle of the aperture between the legs

TT connector nomenclature	h (mm)	α	l_{ab} (mm)	l_t (mm)
TT-12.5-H90-ANG40		40°	95.0	165.0
TT-12.5-H90-ANG50		50°	110.0	180.0
TT-12.5-H90-ANG60	90.0	60°	125.0	195.0
TT-12.5-H90-ANG70		70°	140.0	210.0
TT-12.5-H90-ANG80		80°	155.0	225.0

Table 9 Shear resistance of the TT connector for the different angles between the legs

TT connector	*Pult* (kN)	$Pult_{TT\text{-}12.5\text{-}H90\text{-}ANG60}/Pult$
TT-12.5-H90-ANG40	179.59	1.012
TT-12.5-H90-ANG50	180.13	1.009
TT-12.5-H90-ANG60	181.75	-
TT-12.5-H90-ANG70	182.53	0.996
TT-12.5-H90-ANG80	185.46	0.980

Pult: Shear resistance per TT connector

5.1 Influence of geometric parameters

5.1.1 Height (h)

In order to verify the influence of the connector height on its shear resistance, push-out tests of TT connectors were simulated via the finite element model proposed. The connector has a diameter of 12.5 mm (TT-12.5) and heights of 150 mm, 130 mm, 110 mm, and 90 mm. To maintain the same curvature at the top of the connector to all heights, the ratio h/l_{ab} = 0.72 was kept constant. Table 6 presents the TT connector geometry and their respective nomenclatures. In the push-out numerical model using the 150 mm connector, the height of the slab was enlarged by 15 mm, so that the cover of the connector was preserved. Consequently, this increase was applied to the respective reinforcement bars of the concrete slabs.

Table 7 presents the results of TT connector shear resistance for different heights. There is an increase in shear resistance of 2.77% and a decrease of 4.14% in TT-12.5-H150 and TT-12.5-H90, respectively, compared to TT-12.5-H130. These results enhance the application of TT connector in structures with slabs of small thickness because even with smaller heights, TT connector showed significant shear resistance. In view of this criterion, a TT connector with 90 mm height was selected for continuity of the parametric study.

5.1.2 The angle of the aperture between TT connector legs (α)

In this analysis, push-out models using TT-12.5-H90 connectors were simulated assuming the following values for α: 40º, 50º, 60º, 70º and 80º. The l_t of the connectors was modified varying the α. Table 8 illustrates the geometry and nomenclature of the TT by means of each angle α adopted. Table 9 present the results of the numerical simulations. Assuming TT-12.5-H90-ANG60 as a pattern (ANG meaning the value of α); it was found that it had shear resistance 1.2% higher than TT-12.5-H90-ANG40, and 2.0% lower than TT-12.5-H90-ANG80. Despite the small variation, it was observed that the greater the angle of the aperture between the legs of the TT connector, the greater its shear resistance. Thus, the first step of the parametric study indicated that the height of 90 mm and the angle of 80º between the legs of the TT connector is the geometry that provides greater structural efficiency for the TT connector.

5.2 Influence of connector diameter and concrete strength

At this stage of the parametric study, the influence of the connector diameter (d) and the concrete strength (f_{cm}) in the shear resistance of the TT connector, with a height of 90

Table 10 Simulated push-out models in the second step of the parametric study

Model	TT connector	Diameter (mm)	Concrete strength (MPa)
MTT-8-C25	TT-8-H90-ANG80	8.0	25
MTT-8-C30			30
MTT-8-C35			35
MTT-10-C25	TT-10-H90-ANG80	10.0	25
MTT-10-C30			30
MTT-10-C35			35
MTT-12.5-C25	TT-12.5-H90-ANG80	12.5	25
MTT-12.5-C30			30
MTT-12.5-C35			35

Table 11 Steel properties used in the models of the second step of the parametric study

Parts of the model	Steel properties		
	E_s (GPa)	σ_y (MPa)	σ_u (MPa)
TT connector	210	500	540
Reinforcement of the slab	210	500	-
Beam	200	250	-

Table 12 Concrete properties used in the models of the second step of the parametric study

Concrete properties		
f_{cm} (MPa)	f_{tm} (MPa)	E_0 (GPa)
25	1.99	25.05
30	2.37	26.98
35	2.71	28.77

Table 13 Results of TT connector shear resistance

TT connector	Diameter (mm)	Concrete strength (MPa)	*Pult* (kN)
TT-8-H90-ANG80	8.0	25	67.00
		30	67.39
		35	68.68
TT-10-H90-ANG80	10.0	25	92.73
		30	95.45
		35	96.11
TT-12.5-H90-ANG80	12.5	25	128.20
		30	163.02
		35	170.49

mm and an angle of aperture of 80º, were evaluated. A total of 9 push-out models were simulated, as seen in Table 10. The models were formed by the TT connector, with a diameter of 8.0, 10.0 and 12.5 mm, and concrete, with strength of 25, 30 and 35 MPa. The CA-50 steel properties for the TT connector and reinforcement of the slab were taken from ABNT NBR 6118 (2014) (Table 11) - as Brazilian steel reinforcement bars were used to make the TT connectors in the experiments (Barbosa 2016). The concrete properties are shown in Table 12. The E_0 and f_{tm} were obtained by Eq. (2) and Eq. (9), respectively. The obtained shear resistance values of the connectors can be seen in Table 13 and in Fig. 19.

The results show that the TT-12.5-H90-ANG80 connector, with 35 MPa concrete strength, presented the highest shear resistance of 170.49 kN. The connector that presented the lowest shear resistance (67.00 kN) was the TT-8-H90-ANG80, with concrete strength of 25 MPa. The

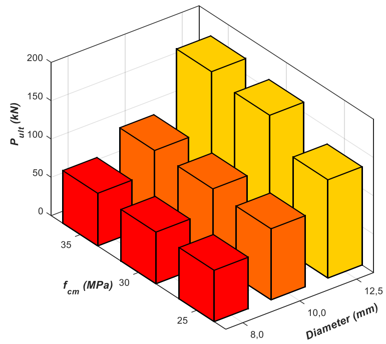

Fig. 19 Illustration of the results of TT connector shear resistance

Table 14 Data considered in the regression analysis

TT connector	Diameter (mm)	A_{TT} (10^{-6} m²)	f_{cm} (MPa)	E_0 (MPa)	Q_{FEA} (kN)
TT-8-H90-ANG80	8.0	100.53	25	25053.52	67.00
			30	26976.43	67.39
			35	28770.52	68.68
TT-10-H90-ANG80	10.0	157.08	25	25053.52	92.73
			30	26976.43	95.45
			35	28770.52	96.11
TT-12.5-H90-ANG80	12.5	245.44	25	25053.52	128.20
			30	26976.43	163.02
			35	28770.52	170.49

Q_{FEA}: Results of TT connector shear resistance from numerical simulation
E_0: Calculated an according to the *fib Model Code 2010* (2012), Eq. (2)

difference between the two opposite shear resistance, the lowest and the highest resistance values, is approximately 154%. In general, the increase of the connector diameter and the concrete strength of the solid slabs increase the shear resistance of the TT connector. It is also known that the variation of the connector diameter has a huge impact on the shear resistance of the TT connector. For the concrete strength of 35 MPa, for example, the increase in the shear resistance was 39.94% between the connectors TT-8-H90-ANG80 and TT-10-H90-ANG80, reaching 148.24% between TT-8-H90-ANG80 and TT-12.5-H90-ANG80 connectors. The increases are similar to the other concrete strength.

Evaluating the variation of the concrete strength of the slabs of the models; it is verified that the influence on the shear resistance of the connectors TT-8-H90-ANG80 and TT-10-H90-ANG80 is not insignificant. Due to the smaller cross sections, the yield in the connectors legs begins before high stress levels are reached in the concrete, thus characterizing the rupture of these models with these connectors, predominantly, by the yield of the legs of the connectors. This fact may be the reason for the low influence of the concrete strength on the shear resistance of these connectors. In the shear resistance of the TT-12.5-H90-ANG80 connector, it is observed a greater dependence of the concrete strength. The increase in its shear resistance was 27.16% and 30.00% when the concrete strength was changed from 25 MPa to 30 MPa and from 25 MPa to 35 MPa, respectively. This TT connector has a higher stiffness; hence, higher stress values are applied to the concrete slab before the yield of the connector legs starts. It has been found that the concrete is more requested and consequently has a greater contribution to the shear resistance of the TT connector with a diameter of 12.5 mm.

6. Equation for TT connector shear resistance prediction

The proposed equation to obtain the TT connector shear resistance was developed from a non-linear regression using statistical software called SPSS v-24.0. Table 14 presents the data, from the numerical simulations performed in the second step of the parametric study, applied in order to make a regression analysis. Based on Ollgaard *et al.* (1971), a potential model was adopted, according to Eq. (18).

$$Q_{TT} = a \cdot \left(A_{TT}\right)^{b} \cdot \left(f_{cm}\right)^{c} \cdot \left(E_0\right)^{d} \tag{18}$$

In Eq. (18), Q_{TT} is the TT connector shear resistance; A_{TT} is the sum of the cross section areas of the two TT connector legs; f_{cm} is the compressive strength of the concrete; and E_0 is the secant modulus of the concrete.

Table 15 Comparison between the calculated values with Eq. (20) and the numerical simulation results

TT connector	f_{cm} (MPa)	Q_{FEA} (kN)	$Q_{Eq.\ (20)}$ (kN)	$Q_{FEA}/\ Q_{Eq.\ (20)}$	*Error (%)*
TT-8-H90-ANG80	25	67.00	55.30	1.212	17.46
	30	67.39	62.85	1.072	6.74
	35	68.68	70.11	0.980	-2.08
TT-10-H90-ANG80	25	92.73	86.40	1.073	6.83
	30	95.45	98.21	0.972	-2.89
	35	96.11	109.55	0.877	-13.98
TT-12.5-H90-ANG80	25	128.20	134.00	0.967	-4.52
	30	163.02	153.45	1.062	5.87
	35	170.49	171.17	0.996	-0.40
Mean				1.022	
Coefficient of variation (CV)				0.093	

Note: *Error (%)* $= 100 \times \left\{ \left(Q_{FEA} - Q_{Eq.(20)} \right) / Q_{FEA} \right\}$

In order to make the regression, 172 statistical models were analyzed. The selection of the equation model that best describes the TT connector shear resistance was based on the correlation coefficient R^2. The following equation (Eq. (19)) presents the best correlation ($R^2 = 0.963$)

$$Q_{TT} = 3.873 \cdot \left(A_{TT} \right)^{0.978} \cdot \left(f_{cm} \right)^{0.412} \cdot \left(E_0 \right)^{0.342} \quad (19)$$

To make easier the application of an equation to find the TT connector resistance, an expression similar to the ones proposed for other connectors in many current standards (AASHTO 2014, AISC 2010, Eurocode-4, 2004) was assumed. Therefore, Eq. (19) was simplified to Eq. (20), a

$$Q_{TT} = 0.695 A_{TT} \sqrt{f_{cm} E_0} \quad (20)$$

Eq. (20) also showed a good agreement with the results of the FE numerical simulations. With a correlation R^2 = 0.959, Eq. (20) is able to describe the nominal resistance of TT connector shear. It is important to point out that Eq. (20) is limited to the TT connector with a height of 90 mm and an angle of the aperture of 80° between its legs and applied to composite steel-concrete beams with a solid slab. An important observation regarding Eq. (20) is that it was developed for nominal resistance. For design practice, Eq. (20) needs reliability studies to define an appropriate safety factor.

Table 15 compares the TT connector shear resistance results from the FE numerical simulation and the proposed Eq. (20). Generally speaking, Table 15 shows that Eq. (20) presents a reasonable agreement with the numerical results. Errors ranging from -4.52% to 6.83% with exception for TT-8-H90-ANG80 with concrete slab with f_{cm} = 25 MPa, and TT-10-H90-ANG80 with concrete slab with f_{cm} = 35 MPa. Despite these two exception, the average value of ($Q_{FEA}/Q_{Eq.(20)}$) was 1.022, with a variation coefficient of 0.093.

7. Conclusions

In this research, an alternative Truss Type (TT) shear connector for composite concrete-steel beams was studied. TT connectors were experimentally studied with standard push-out tests and, compared to headed stud bolts, showed higher resistance for shear, slipping, and uplift. Moreover, such connectors can be produced with low cost, and their installations do not require specific welding equipment like stud guns operated with high electric power. However, more studies for this new type of connector are still needed. This article presented a parametric study evaluating the shear resistance of the TT connectors. For such, numerical simulations using three-dimensional nonlinear finite element (FE) models were developed using the software ABAQUS. In the parametric study, the variation of the TT connector height, the angle of the aperture between the connector legs, the connector diameter, and the concrete strength of the solid slabs were evaluated numerically with FE simulations of push-out tests. The FE models considered the nonlinearities associated with concrete and steel materials. The concrete damage plasticity model was adopted to simulate the complex behavior of the concrete in the push-out test models. In the analyses, the explicit dynamic method was quite effective, simulating the complex nonlinearities imposed by the contact interactions between the TT connector and concrete slab in the FE models. Both the load-slip curves and the modes of rupture numerically obtained were very consistent with the experimental results available in the literature. The parametric study showed that the TT connector with a height of 90 mm and an angle of aperture of 80° was the one that presented the highest structural efficiency for concrete with 25, 30, and 35 MPa of compressive strength. Regarding the height variation, it was observed that the greater the height of the TT connector, the greater is its shear resistance. However, quantitatively speaking, the TT connector shear resistance values varied slightly since the rupture took place at its base or in the slab regions near the

TT connector. As the TT connector shear resistance is little affected by its height variation, it has great potential for application in composite structures with slabs of small thickness. The increase in the angle of the aperture between the legs of the TT connector produces an increase in its shear resistance. The increase in the concrete strength and in the diameter of the TT connector generated improvements in the TT connector shear resistance. Based on statistical analysis of the parametric study, a practical equation to predict the nominal shear resistance of the TT connector was suggested. However, reliability studies are necessary to provide an appropriate safety factor for design practice. The finite element model developed, as well as the results of this research contributed to a better understanding of the structural behavior of the new Truss Type shear connector, thus collaborating for its future applications.

Acknowledgments

The authors would like to thank CAPES (the Brazilian Coordination for the Improvement of Higher Education Personnel) and CNPq (the National Council for Scientific and Technological Development) for the financial supports for this research.

References

AASHTO (2014), Load and Resistance Factor Design (LRFD) Bridge design specifications, (7th Edition); American Association of State Highway and Transportation Officials, Washington, D.C., USA.

AISC (2010), Load and Resistance Factor Design (LRFD) Specification for Structural Steel Building; American Institute of Steel Construction, Chicago, IL, USA.

ABAQUS (2014-a), User's Manual, Version 6.14-1, Dessault Systèmes Simulia Corp, Provice, RI, USA.

ABAQUS (2014-b), Theory Manual, Version 6.14-1, Dessault Systèmes Simulia Corp, Provice, RI, USA.

ABNT NBR 6118 (2014), Design of concrete structures – Procedure, Brazilian Association for Technical Standards, Rio de Janeiro, Brazil (In Portuguese).

Alfarah, B., López-Almansa, F. and Oller, S. (2017), “New methodology for calculating damage variables evolution in Plastic Damage Model for RC structures”, *Eng. Struct.*, **132**, 70-86. https://doi.org/10.1016/j.engstruct.2016.11.022.

Araújo, D. de L., Sales, M.W.R., Paulo, S.M. de and Debs, A.L.H. de C. El. (2016), “Headed steel stud connectors for composite steel beams with precast hollow-core slabs with structural topping”, *Eng. Struct.*, **107**, 135-150. https://doi.org/10.1016/j.engstruct.2015.10.050.

Ban, H., Bradford, M.A., Uy, B. and Liu, X. (2016), “Available rotation capacity of composite beams with high-strength materials under sagging moment”, *J. Constr. Steel Res.*, **118**, 156-168. https://doi.org/10.1016/j.jcsr.2015.11.008.

Barbosa, W.C.S. (2016), “Study of steel rebar shear connector for steel-concrete composite beams”, Ph.D. Thesis Dissertation, The University of Brasília, Brasília (In Portuguese).

Bezerra, L.M., Barbosa, W.C.S., Bonilla, J. and Cavalcante, O.R.O. (2018), “Truss-type shear connector for composite steel-concrete beams”, *Constr. Build. Mater.*, **167**, 757-767. https://doi.org/10.1016/j.conbuildmat.2018.01.183.

Bonilla, J., Bezerra, L.M., Mirambell, E. and Massicotte, B. (2018), “Review of stud shear resistance prediction in steel-concrete composite beams”, *Steel Compos. Struct.*, **27**(3), 355-370. https://doi.org/10.12989/scs.2018.27.3.355.

Cândido-Martins, J.P.S., Costa-Neves, L.F. and Vellasco, P.C.G.d. S. (2010), “Experimental evaluation of the structural response of Perfobond shear connectors”, *Eng. Struct.*, **32**(8), 1976-1985. https://doi.org/10.1016/j.engstruct.2010.02.031.

Cornellissen H., Hordijk D. and Reinhardt, H. (1986), “Experimental determination of crack softening characteristics of normal weight and lightweight concrete”, *Heron*. **31** 45-56.

Ellobody, E. and Young, B. (2006), “Performance of shear connection in composite beams with profiled steel sheeting”, *J. Constr. Steel Res.*, **62**(7), 682-694. https://doi.org/10.1016/j.jcsr.2005.11.004.

Eurocode-4 (2004), Design of Composite Steel and Concrete Structures Part 1.1; European Committee for Standardization, Brussels, Belgium.

fib Model Code 2010, (2012), *fib Model Code* 2010 Final *draft* Volume 2, The International Federation for Structural Concrete, Lausanne, Switzerland.

Han, Q., Wang, Y., Xu, J., Xing, Y. and Yang, G. (2017), “Numerical analysis on shear stud in push-out test with crumb rubber concrete”, *J. Constr. Steel Res.*, **130**, 148-158. https://doi.org/10.1016/j.jcsr.2016.12.008.

Kim S.H., Park, S., Kim, K.S. and Jung, C.Y. (2017), “Generalized formulation for shear resistance on Y-type perfobond rib shear connectors”, *J. Constr. Steel Res.*, **128**, 245-260. https://doi.org/10.1016/j.jcsr.2016.08.016.

Kim, S.H., Kim, K.S., Park, S., Ahn, J.H. and Lee, M.K. (2016), “Y-type perfobond rib shear connectors subjected to fatigue loading on highway bridges”, *J. Constr. Steel Res.* **122**, 445-454. https://doi.org/10.1016/j.jcsr.2016.04.015.

Krätzig, W.B. and Pölling R. (2004), “An elasto-plastic damage model for reinforced concrete with minimum number of material parameters”, *Comput. Struct.*, **82**(15-16), 1201-1215. https://doi.org/10.1016/j.compstruc.2004.03.002.

Lam, D. (2007), “Capacities of headed stud shear connectors in composite steel beams with precast hollowcore slabs”, *J. Constr. Steel Res.*, **63**(9), 1160-1174. https://doi.org/10.1016/j.jcsr.2006.11.012.

Lam D. and El-Lobody, E. (2005), “Behavior of headed stud shear connectors in composite beam”, *J. Struct. Eng.*, **131**(1), 96-107. https://doi.org/10.1061/(ASCE)0733-9445(2005)131:1(96).

Lopez-Almansa, F., Alfarah, B. and Oller, S. (2014), “Numerical simulation of RC frame testing with damaged plasticity model comparison with simplified models”, *Proceedings of the Conference: 2nd European conference on earthquake engineering and seismology*, Istanbul, Turkey, August.

Nguyen, H.T. and Kim, S.E. (2009b), “Finite element modeling of push-out tests for large stud shear connectors”, *J. Constr. Steel Res.*, **65**(10-11), 1909-1920. https://doi.org/10.1016/j.jcsr.2009.06.010.

Oller S. (1988), “A Continuous damage model for frictional materials”. Ph.D. Thesis Dissertation. Technical University of Catalonia, Barcelona.

Ollgaard, J.G., Slutter, R.G. and Fisher, J.W. (1971), “Shear Strength of Stud Connectors in Lightweight and Normal-Weight Concrete”, *Eng. J. AISC*, **8**(2), 55-64.

Paknahad, M., Shariati, M., Sedghi, Y., Bazzaz, M. and Khorami, M. (2018), “Shear capacity equation for channel shear connectors in steel-concrete composite beams”, *Steel Compos. Struct.*, **28**(4), 483-494. https://doi.org/10.12989/scs.2018.28.4.483.

Pavlović, M., Marković, Z., Veljković, M. and Buđevac, D. (2013), “Bolted shear connectors vs. headed studs behaviour in push-out tests”, *J. Constr. Steel Res.*, **88**, 134-149. https://doi.org/10.1016/j.jcsr.2013.05.003.

Qi, J., Wang, J., Li, M. and Chen, L. (2017), “Shear capacity of stud shear connectors with initial damage: Experiment, FEM model and theoretical formulation", *Steel Compos. Struct.*, **25**(1), 79-92. https://doi.org/10.12989/scs.2017.25.1.079.

Qureshi, J. and Lam, D. (2012), "Behaviour of headed shear stud in composite beams with profiled metal decking", *Adv. Struct. Eng.*, **15**(9), 1547-1558. https://doi.org/10.1260/1369-4332.15.9.1547.

Qureshi, J., Lam, D. and Ye, J. (2011), "The influence of profiled sheeting thickness and shear connector's position on strength and ductility of headed shear connector", *Eng. Struct.*, **33**(5), 1643-1656. https://doi.org/10.1016/j.engstruct.2011.01.035.

Shariati, M., Ramli Sulong, N.H., Shariati A. and Khanouki, M.A. (2016), "Behavior of V-shaped angle shear connectors: experimental and parametric study", *Mater. Struct.*, **49**(9), 3909-3926. https://doi.org/10.1617/s11527-015-0762-8.

Turmo, J., Lozano-Galant, J. A., Mirambell, E. and Xu, D. (2015), "Modeling composite beams with partial interaction", *J. Constr. Steel Res.*, **114**, 380-393. https://doi.org/10.1016/j.jcsr.2015.07.007.

Veríssimo, G.S., Paes, J.L.R., Valente, I., Cruz, P.J.S. and Fakury, R.H. (2006), "Design and experimental analysis of a new shear connector for steel and concrete composite structures", *Proceedings of the 3rd Int. Conf. Bridg. Maintenance, Saf. and Manag.*, Porto, Portugal, July.

Xing, Y., Han, Q., Xu, J., Guo, Q. and Wang, Y. (2016), "Experimental and numerical study on static behavior of elastic concrete-steel composite beams", *J. Constr. Steel Res.*, **123**, 79-92. https://doi.org/10.1016/j.jcsr.2016.04.023.

Xu, X., Liu, Y. and He, J. (2014), "Study on mechanical behavior of rubber-sleeved studs for steel and concrete composite structures", *Constr. Build. Mater.*, **53**, 533-546. https://doi.org/10.1016/j.conbuildmat.2013.12.011.

Zheng, S., Liu, Y., Liu, Y. and Zhao, C. (2019), "Experimental and parametric study on the pull-Out resistance of a notched perfobond shear connector", *Appl. Sci.*, **9**(4), 1-20. https://doi.org/10.3390/app9040764.

Zona, A. and Ranzi, G. (2014), "Shear connection slip demand in composite steel–concrete beams with solid slabs", *J. Constr.Steel Res.*, **102**, 266-281. https://doi.org/10.1016/j.jcsr.2014.07.018.

DL